Supporting Information

Tsuji *et al.* 10.1073/pnas.0804277105

SI Text

Results and Discussion. ***Nucleation and formation of crystalline calcium phosphate in the presence of artificial proteins (#64 and #68) and control proteins.*** We observed that clones with higher acceleration indices had the distinct ability to form crystalline calcium phosphate under conditions that otherwise do not allow crystal formation, even after incubation for 10 days. We examined precipitates from calcium phosphate solutions [1.8 mM $CaCl_2$, 1.08 mM KH_2PO_4 (pH 7.4) 25 °C] in the absence and presence of different concentrations (200, 40, 8, and 1.6 μg/ml) of artificial proteins (#56, #64, #68, and #69) and control proteins (GST-DMP1, mixture of pA and pB, phosvitin, BSA, lysozyme, polyAsp, and polyLys). After incubation for 10 days, only small amounts of an irregularly shaped precipitate were obtained from solutions not containing a protein (Fig. S2*A*) or containing protein #56 or #69, or any of the control proteins, at the aforementioned concentrations. However, large amounts of a spherical precipitate were obtained from solutions containing 40 μg/ml #64 or #68 after incubation for only 5 days (Fig. S2 *B–E*). Protein #64 accelerated the precipitation at a concentration of 1.6 μg/ml, although a higher concentration of #68 was required (Table S1), which is consistent with the results of our pH-drop experiments. This spherical precipitate was made up of aggregates of blade-shaped crystals. Using energy dispersive X-ray (EDX) analysis, the Ca/P ratio of these crystals was determined to be 1.30 ± 0.07 (n = 11), which is consistent with the chemical formula for octacalcium phosphate [OCP; $Ca_8H_2(PO_4)_6{\cdot}5H_2O$]. The X-ray diffraction (XRD) spectra also showed the aggregates to be OCP, as indicated by the (010) reflection at 4.7°, (002) reflection at 26°, and reflections around 32° (Fig. S2*F*). Thus, #64 and #68 enhanced nucleation and formation of OCP under the conditions used. Calcium phosphate precipitated from neutral or basic solutions is usually HAP or OCP, depending on the pH of the solutions. That OCP was obtained under our conditions is consistent with earlier reports (1, 2).

Nucleation and formation of crystalline calcium phosphate in the presence of #64 derivatives. We constructed 4 #64 mutants (#64A, #64B1, #64B2, and #64B3) in which the acidic residues in a peptide motif (motif A or motif B) were mutated to glutamines and/or asparagine (*SI Materials and Methods*, below). Subsequent pH-drop experiments showed that the ability of these mutants to accelerate crystal formation was significantly reduced at a low protein concentration (1 μg/ml) (Fig. S1). Spherical aggregates of calcium phosphate were obtained only from solutions containing a relatively high concentration (40 and/or 200 μg/ml) of the #64 mutants (Table S1), which indicates that the acceleration activity required the presence of the embedded motifs.

Time-resolved static light-scattering (TR-SLS) measurements of calcium phosphate formation in the presence of DMP1. We carried out TR-SLS measurements using solution containing 25 μg/ml GST-DMP1 (Fig. S4). As suggested by a previous report (3) and our pH measurements (Fig. 3 in the main text), DMP1 delayed precipitation considerably. The particle size at the initial stage of the precipitation reaction was considerably smaller than that at the same stage of the reaction in the absence of this protein (see Fig. 4 in the main text; R_g = 75–100 nm versus 350–400 nm). This indicates that excess of the acidic residues in the DMP1 chelated calcium ions, which lowered the degree of super saturation. Acceleration activity of the DMP1 motifs thus was hindered in the full-length DMP1 when this protein was added to the solution without immobilization.

Structural properties of representative artificial proteins. We obtained the circular dichroism (CD) spectra for #64 in the presence and absence of calcium ion. These spectra did not show a distinct minimum at ≈222 nm or 215 nm (Fig. S5), indicating that the protein does not form secondary structures such as α-helix or β-sheet. Thus, a folded conformation is not required for the protein to accelerate crystal formation. Moreover, the calcium ion did not alter the conformation of the proteins. We also made dynamic light-scattering (DLS) measurements of the protein and found the hydrodynamic radius (R_H) to be ≈3 nm, indicating that the protein was present in a monomeric or small oligomeric state under the conditions used.

Materials and Methods. ***Construction and purification of artificial proteins.*** The artificial proteins were created by using MolCraft (4). First, a 68-bp microgene (MG-69) was designed so that it encoded motif-A (QESQSEQDS) and motif-B (ESQES) (5) in its first and second reading frames, respectively. We also embedded the mini-titanium-binding peptide (minTBP-1, RKLPDA) (6) in the third reading frame for future experiments (Fig. S6). By using CyberGene (4), the microgene's codons were selected so that the peptides encoded would be hydrophobic. The designer microgene was then tandemly polymerized by using MPR (microgene polymerization reaction) (7, 8) by reacting two MPR primers, KY-1473 (5′-CTCGCAAGCTTCCCGACGCTCCGAATCGCAGGAATCGGT-3′) and KY-1474 (5′-TGAGAATCCTGCTCCGACTGAGACTCCTGTCCGATTCCTGCGT-3′), with Vent DNA polymerase (New England BioLabs) and dNTP. The reactions were run without a DNA template for 50 cycles. Note that the primers have a mismatched pair at their 3′-OH ends; this has been shown to enhance polymerization (4). The obtained microgene polymers were ligated at the SmaI site of pTZ19R, as described previously (9), and sequenced. During the polymerization reaction, insertion and deletion mutations occurred randomly at the end-joining junctions between the microgenes. Consequently, the resultant polymers made up a library whose coding sequences were composed of combinatorial polymers of the three reading frames from a single microgene. Because the two DMP1 motifs were embedded in different reading frames, we were able to prepare artificial proteins that had various numbers of the 2 motifs in different orders (Fig. S7a). To express the proteins, BamHI-*Asp*718 fragments containing the polymers were subcloned into the BglIII-Asp718 sites of expression vectors (pKS600+, pKS601+, pKS602+, pKS604+, pKS605+, and pKS 606+) in which a Trp residue was introduced after the 6× His-tag portion at the N terminus of the encoded fusion protein. The proteins were then expressed in *E. coli* K12 strain XL1Blue (Strategene) and purified by using TALON resin (Clontech) under denaturing conditions, as described previously. All artificial proteins purified were extensively dialyzed against 10 mM KH_2PO_4 (pH 8.0), and proteins #56, #64, #68, and #69 were further dialyzed against 1 mM HCl. The results of SDS/PAGE of the purified proteins is shown in Fig. S7*B*. The molecular masses of #56, #64, #68, and #69 were confirmed by mass spectroscopy (data not shown). Molar concentrations of the proteins were determined by absorbance at 280 nm.

Construction of derivatives of #64. Because the gene encoding #64 consisted of tandem repeats of a microgene, we were unable to use a conventional mutagenesis technique to introduce mutations into the gene. We therefore constructed mutant derivatives of #64 by redesigning the DNA sequences and reconstituting the DNA from three minigene blocks. In this process, we chose codons that reduced the repetitiveness of the genes because this

was necessary to reconstitute the genes. Each minigene was prepared by PCR using a pair of oligonucleotides in which the 3′ regions overlapped. Because the resultant minigenes had overlapping regions, we were able to assemble the whole gene using overlapped extension PCR (10), after which the sequences of the assembled genes were confirmed by DNA sequencing. Proteins were expressed and purified as described above, and the molecular masses of the mutant proteins were confirmed by mass spectroscopy. The oligonucleotides used for construction of the mutants were as follows (see Table S2 for numbering the oligonucleotides). ⟨1–108(+)⟩ 5′-CATCACCATACGGATCCGTCGACTTGGGCAGATCCCCGACGCTCCGAATCGCAGGAATCGGACAGGAGTCTCAGTCGGAGCAGGATTCTCACTCGTAAACTGCCGGAT-3′, ⟨1–108(+)A⟩ 5′-CATCACCATACGGATCCGTCGACTTGGGCAGATCCCCGACGCTCCCAGTCGCAGCAGTCGGACAGGAGTCTCAGTCGGAGCAGGATTCTCACTCGTAAACTGCCGGAT-3′, ⟨79–186(−)⟩ 5′-CGCAATGCGCAGGGTTGGAAACGACGCCGA AAAACCGGCGCCAACGGAAACACCGGTGCGGTTGCGACGGTTTGGCGCATC CGGCAGTTTACGAGTGAGAATCCTGCT-3′, ⟨163–270(+)⟩ 5′-TCGTTTCCAACC CTGCGCATTGCGGGCATTGGCCAAGAAAGCCAGAGTGAACAAGACAGCCTGGCCAGCTTCCCGACGCTTCGTATCGCCGGTATCGGTCAGGAGAGT-3′, ⟨163–270(+)B1⟩ 5′-TCGTTTCCAACCCTGCGCATTGCGGGCATTGGCCAACAGAGCCAGAGTCAGCAAAACAGCCTGGCCAGCTTCCCGACGCTTCGTATCGCCGGTATCGGTCAGGAGAGT-3′, ⟨163–270(+)B2⟩ 5′-TCGTTTCCAACCCTGCGCATTGCGGGCATTGGCCAAGAAAGCCAGAGTGAACAAGACAGCCTGGCCAGCTTCCCGACGCTTCGTATCGCCGGTATCGGTCAGCAAAGT-3′, ⟨247–357(−)⟩ 5′- GAGCGAGTCCTGCTCACTTTGCGATTCCTGCCCAATCCCTGCAATCCGGAGAGTAGGGAAGGATGCATGAGAATCCTGTTCCGATTGACTCTCCTGACCGATACCGGCGAT-3′, ⟨247–357(−)B2⟩ 5′-GAGCGAGTCCTGCTCACTTTGCGATTCCTGCCCAATCCCTGCAATCCGGAGAGTAGGGAAGGATGCATGAGAGTTCTGTTGCGATTGACTTTGCTGACCGATACCGGCGAT-3′, ⟨247–357(−)B3⟩ 5′-GAGCGAATTCTGTTGACTTTGCGACTGCTGCCCAATCCCTGCAATCCGGAGAGTAGGGAAGGATGCATGAGAATCCTGTTCCGATTGACTCTCCTGACCGATACCGGCGAT-3′, ⟨331–438(+)⟩ 5′-GAATCGCAAAGTGAGCAGGACTCGCTCGCCTCCTTTCCCACGCTGCGTATCGCTGGCATCGGGCAAGAGTCTCAGTCCGAAGGGTACCCGGGTTAATTAATTAACTAG-3′, ⟨331–438(+)B3⟩ 5′-CAGTCGCAAAGTCAACAGAATTCGCTCGCCTCCTTTCCCACGCTGCGTATCGCTGGCATCGGGCAAGAGTCTCAGTCCGAAGGGTACCCGGGTTAATTAATTAACTAG-3′, ⟨pri1–108(+)⟩ 5′-CATCACCATACGGATCCGTCGACT-3′, ⟨pri79–186(−)⟩ 5′-CGCAATGCGCAGGGTTGGAAACGA-3′, ⟨pri163–270(+)⟩ 5′-TCGTTTCCAACCCTGCGCATTGCG-3′, ⟨pri247–357(−)⟩ 5′-GAGCGAGTCCTGCTCACTTTGCGATTC-3′, ⟨pri247–357(−)B3⟩ 5′-GAGCGAATTCTGTTGACTTTGCGACTG-3′, ⟨pri331–438(+)⟩ 5′-GAATCGCAAAGTGAGCAGGACTCGCTC-3′, ⟨pri331–438(+)B3⟩ 5′-CAGTCGCAAAGTCAACAGAATTCGCTC-3′, and ⟨pri331–438(+)*r*⟩ 5′-CTAGTTAATTAATTAACCCGGGTACCCTTC-3′.

Monitoring pH as an index of HAP precipitation. Solutions of $CaCl_2$ and KH_2PO_4 were freshly prepared by using reagent grade materials (Wako) and MilliQ water (Biocel A10; Millipore), after which they were filtered through a 0.2-μm Millipore filter (Millex-GN; Millipore). Artificial proteins, GST-DMP1, BSA (albumin bovine Cohn Fraction V; Iwai Chemical), Phosvitin (from egg yolk; Sigma), and lysozyme (from chicken egg white; Sigma) were extensively dialyzed against 10 mM KH_2PO_4 (pH 8.0) before the experiments. GST-DMP1 was constructed as reported previously (11). Stock solutions of the pA and pB peptides (Any Gen), polyAsp (molecular mass 15,000–50,000 kDa; Sigma), and polyLys (molecular mass 15,000–30,000 kDa; Sigma) were prepared by dissolving them in 10 mM KH_2PO_4 (pH 8.0) to a concentration of 1 mg/ml. Before the reaction, selected amounts of artificial protein or reference additive were dissolved in 1,360 μl of KH_2PO_4 (5.0 mM, pH 8.0). The mineralization reactions were started by mixing the KH_2PO_4 solution with 140 μl of 21.3 mM $CaCl_2$ in a 2.0-ml plastic tube (Eppendorf) by using a magnet bar (6.35 × 3 mm) for stirring. The pH of the solution was then recorded every 1.5 s by using a pH meter (model F22; Horiba). The reactions were run at a constant temperature of 25 °C (Cool Stirrer SWC-900; Nissin), and all solutions were equilibrated to that temperature before the reactions were started.

To characterize the precipitates by using XRD and TEM, the reactions were scaled up to 30 ml, which did not alter the pH-drop profiles of the reactions. The precipitates were recovered by centrifugation at the indicated times, rinsed with MilliQ water, and then freeze-dried, after which the samples were analyzed by using an X-ray powder diffractometer (RINT 2500, 56 kV, 200 mA, CuKα; Rigaku). In addition, the morphologies of the precipitates were examined by TEM, H7600; Hitachi High Technologies) at 100 kV.

TR-SLS measurements. The details of the instrument were described previously (12). Briefly, an ellipsoidal mirror and a high-speed CCD camera enables simultaneous collection of the scattered light from a wide range of scattering angles. As a result, TR-SLS has higher temporal and spatial (in terms of scattering angle) resolutions than conventional SLS: The angular dependence of the scattering intensity can be simultaneously obtained at angles ranging from 10° to 170° within a time interval of 1 s with a maximum angular resolution of 1°. A 10-mW He-Ne laser was used as the light source for the SLS measurements (λ_w = 632.8 nm).

The calcium phosphate solution used for transformation experiments contained 2.5 mM KH_2PO_4 (adjusted to pH 8.0 by NaOH) and 1.0 mM $CaCl_2$, and the measurements were made at a constant temperature of 25 °C. The apparent molecular mass (M_w) and gyration radius (R_g) were calculated using a Zimm-Square plot (12, 13). The scattering intensity of the calcium phosphate solution in excess to the solvent scattering was expressed by using excess Rayleigh ratio $\Delta R(q)$:

$$\{Kc/\Delta R(q)\}^{1/2} = [1/\{M_w P(q)\}]^{1/2}(1 + A_2 M_w c). \quad [1]$$

In this Zimm-square equation, K is the system-specific constant, c is the concentration, $P(q)$ is the form factor and A_2 is the second virial constant of calcium phosphate. K is expressed by using the solvent refractive index n_0, incident light wavelength λ_w, Avogadro's number N_A, and refractive index increment dn/dc of the calcium phosphate solution:

$$K = 4\,\pi^2 n^2/(N_A \lambda_w)(dn/dc)^2. \quad [2]$$

The scattering vector q is expressed using the scattering angle θ:

$$q = 4\pi\, n_0/\lambda_w \sin(\theta/2). \quad [3]$$

The q range we used in the SLS measurement was $0.794 \le q \le 2.392$ (10^{-2} nm^{-1}).

Eq. **1** can be rewritten into a form using R_g of the aggregates as

$$\{Kc/\Delta R(q)\}^{1/2} = (1/M_w)^{1/2}(1 + R_g^2 q^2/6). \quad [4]$$

The contribution of $A_2 c$ was neglected, as is commonly done in time-resolved SLS measurements (12, 13). The M_w and R_g were determined from a plot of $\{Kc/\Delta R(q)\}^{1/2}$ vs. q^2 at the extrapolated limit of zero q. The obtained M_w was thus the apparent value.

The fractal dimension d_f reflects the compactness and regularity of the inner structure of the aggregate. It is calculated from the relationship between the scattering intensity and the scat-

tering vector $I(q) \approx q^{-d}$ when the relationship $1/R_g < q < 1/r_H$ (monomer of calcium phosphate) is held.

Formation and characterization of calcium phosphate crystals. Artificial proteins and reference materials (lysozyme, BSA, and phosvitin) were dialyzed against 1 mM HCl and freeze-dried, whereas GST-DMP1 was dialyzed against 1% ammonia solution and freeze-dried. The dried materials (including polyAsp, polyLys, and the synthetic peptides pA and pB, which were provided in dried form) were dissolved in 500 μl of 2.16 mM KH_2PO_4 to final concentrations of 400, 80, 16, and 3.2 μg/ml. The pH of the solutions was then adjusted to 7.4 by using NaOH or HCl, after which an equal volume of 3.6 mM $CaCl_2$ was added to start the precipitation reaction. After incubating the reaction mixture for 5 or 10 days at 25 °C, the solutions were filtered through a polycarbonate membrane (pore size, 0.2 μm; Isopore membrane filter; Millipore) to collect the precipitate, which was then air-dried and analyzed by using SEM (VE-8800; KEYENCE) and XRD (RINT 2500, 56 kV, 200 mA, CuKα; Rigaku). For the XRD analysis, 21 ml of reaction solution was used.

To observe cross-sections of a particle, the precipitants were embedded in epoxy resin (Epon 812 resin; TAAB Laboratories Equipment), sliced into ultrathin (200-nm) sections, and analyzed by TEM/EDX (TEM, H7600; Hitachi High Technologies; HORIBA, EMAX ENERGY) and TEM/SAED.

Structural analysis of artificial proteins. Far-UV CD spectra of #64 in 50 mM Tris·HCl (pH 8.0) were measured in the presence and absence of 5 mM calcium ion at 25 °C by using a Jasco spectropolarimeter (model J-820) fitted with a thermostatted cell holder. The protein concentration was 400 μg/ml. The DLS measurements were made by using a DynaPro (Protein Solution) at 25 °C. The protein concentration was 1 mg/ml.

1. Ofir PBY, Govrin-Lippman R, Garti N, Füredi-Milhofer H (2004) The influence of polyelectrolytes on the formation and phase transformation of amorphous calcium phosphate. *Cryst Growth Des* 4:177–183.
2. Tarasevich BJ, *et al.* (2007) The nucleation and growth of calcium phosphate by amelogenin. *J Cryst Growth* 304:407–415.
3. He G, *et al.* (2005) Spatially and temporally controlled biomineralization is facilitated by interaction between self-assembled dentin matrix protein 1 and calcium phosphate nuclei in solution. *Biochemistry* 44:16140–16148.
4. Shiba K (2004) MolCraft: A hierarchical approach to the synthesis of artificial proteins. *J Mol Catalysis B* 28:145–153.
5. He G, Dahl T, Veis A, George A (2003) Nucleation of apatite crystals in vitro by self-assembled dentin matrix protein 1. *Nat Mater* 2:552–558.
6. Sano K, Shiba K (2003) A hexapeptide motif that electrostatically binds to the surface of titanium. *J Am Chem Soc* 125:14234–14235.
7. Shiba K, Takahashi Y, Noda T (1997) Creation of libraries with long open reading frames by polymerization of a microgene. *Proc Natl Acad Sci USA* 94:3805–3810.
8. Shiba K, Takahashi Y, Noda T (2002) On the role of periodism in the origin of proteins. *J Mol Biol* 320:833–840.
9. Shiba K, Minamisawa T (2007) A synthesis approach to understanding repeated peptides conserved in mineralization proteins. *Biomacromolecules* 8:2659–2664.
10. Horton RM, Hunt HD, Ho SN, Pullen JK, Pease LR (1989) Engineering hybrid genes without the use of restriction enzymes: Gene splicing by overlap extension. *Gene* 77:61–68.
11. George A, Sabsay B, Simonian PA, Veis A (1993) *J Biol Chem* 268:12624–12630.
12. Onuma K, *et al.* (2000) Precipitation kinetics of hydroxyapatite revealed by the continuous-angle laser light-scattering technique. *J Phys Chem B* 104:10563–10568.
13. Onuma K (2005) Effect of phosvitin on the nucleation and growth of calcium phosphates in physiological solutions. *J Phys Chem B* 109:8257–8262.

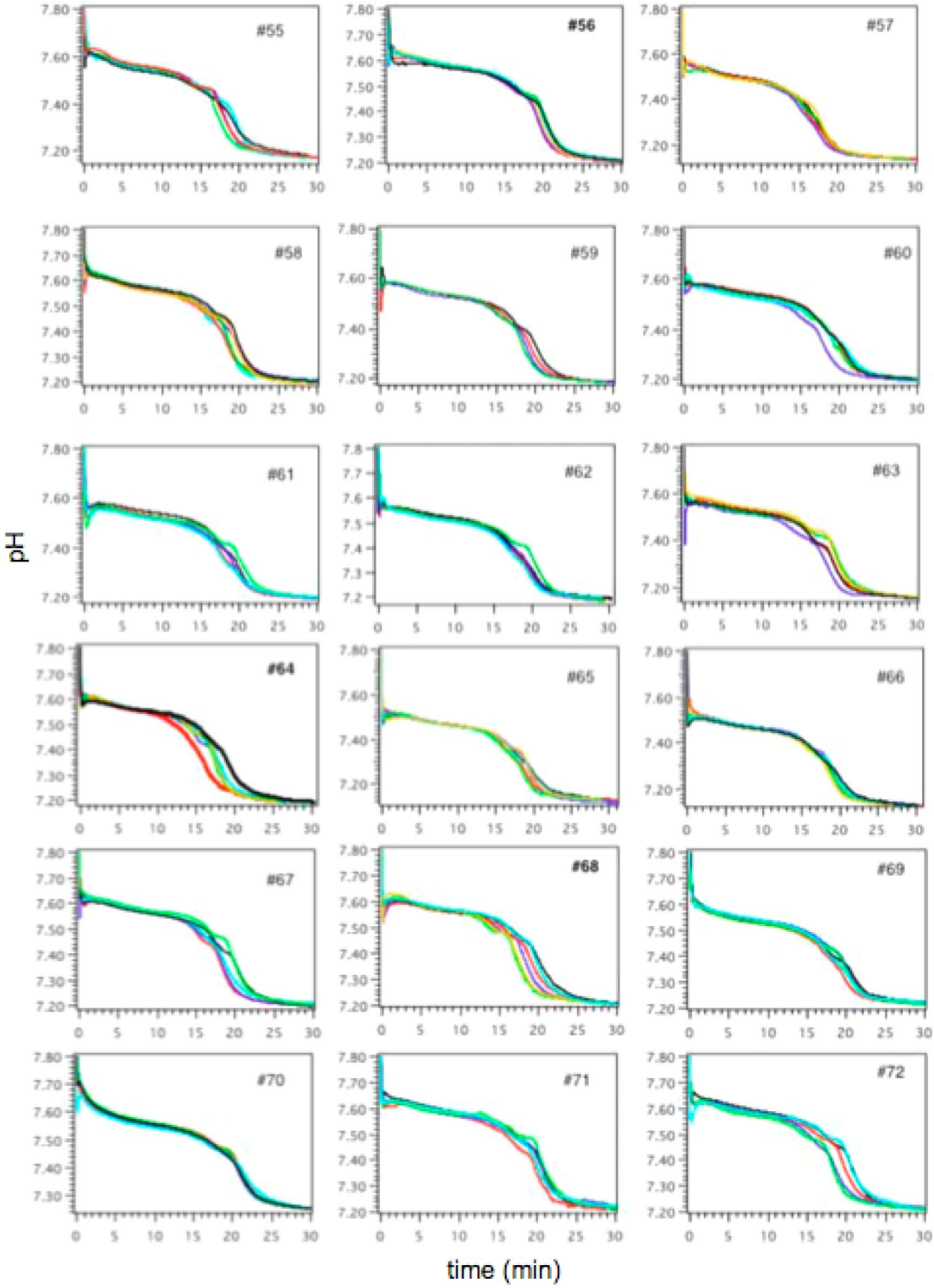

Fig. S1. pH-drop profiles in the presence of artificial proteins. pH changes were measured in the presence of different concentrations of the indicated proteins (sky blue, 0.2; red, 1; blue, 5; green 25; orange, 125 μg/ml). The profiles with the #64 mutants (#64A, #64B1, #64B2, and #64B3) are also indicated. Acceleration indices for the four #64 mutants at 1 and 25 μg/ml are indicated.

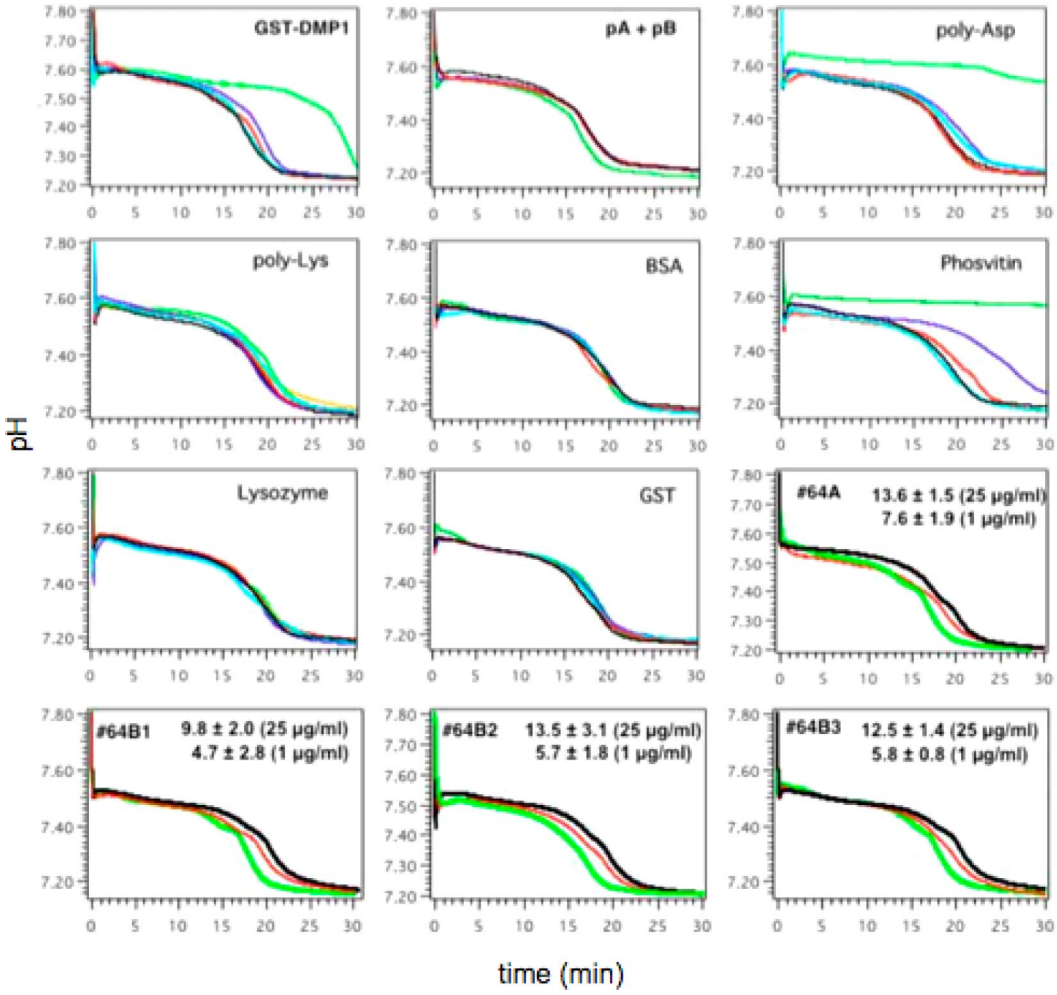

Fig. S1 ***continued.***

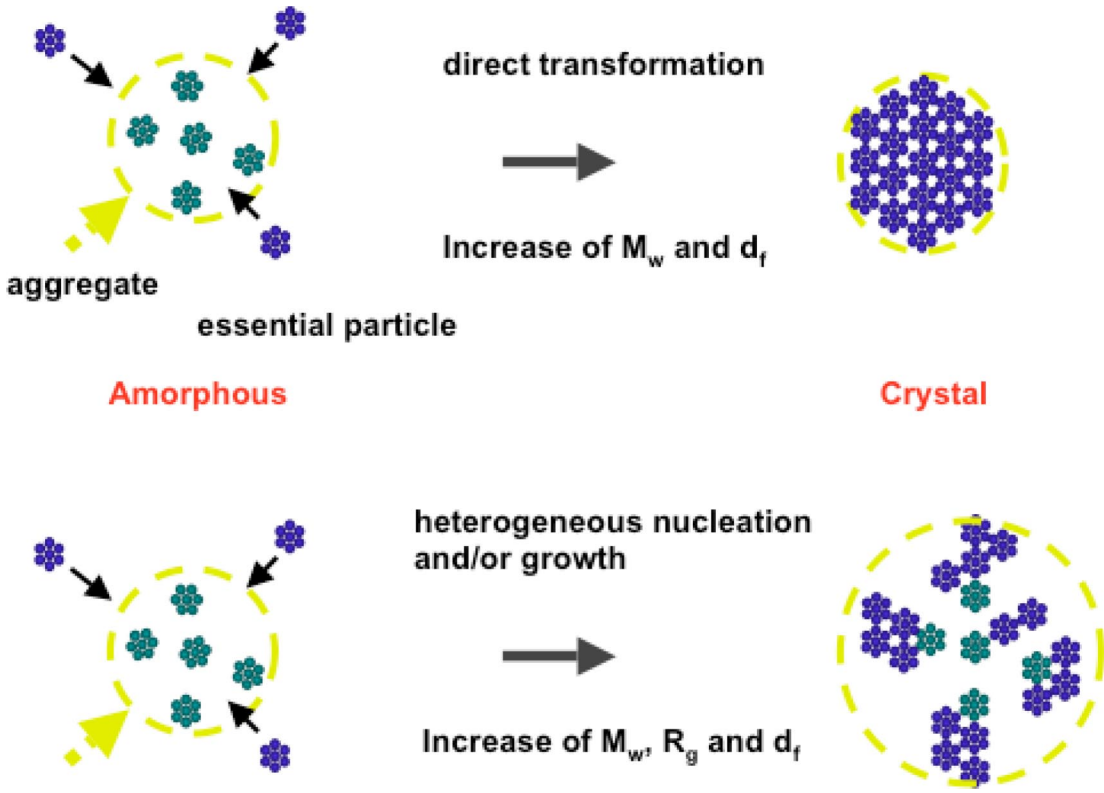

Fig. S2. SEM and TEM images of calcium phosphate formed with #64. Precipitation from a solution of 1.8 mM $CaCl_2$ and 1.08 mM KH_2PO_4 (pH7.4) in the presence and absence of #64. (*A*) Precipitate after incubation for 10 days without protein. Control samples, #56, #69, GST-DMP1, mixture of pA and pB, phosvitin, BSA, lysozyme, polyAsp, and polyLys all gave the similar results (data not shown). (*B–E*) Precipitate after incubation for 5 days with 40 μg/ml #64. The diameters ranged from 5–50 μm, and the blades were 2–5 μm wide and $\approx$0.1 μm thick. The blade-like morphology is a feature of octacalcium phosphate (OCP) crystals, which consist of large (100) faces elongated along the *c* axis and terminated by (011) faces. (*F*) X-ray diffraction (XRD) spectra of calcium phosphate particles formed in the presence of #64. Particles were collected from a polycarbonate membrane. An XRD spectrum of a polycarbonate membrane alone is also shown (*Inset*). (Scale bars: *A*, 50 μm; *B*, 50 μm; *C*, 20 μm; *D*, 1 μm; and *E*, 2.5 μm.)

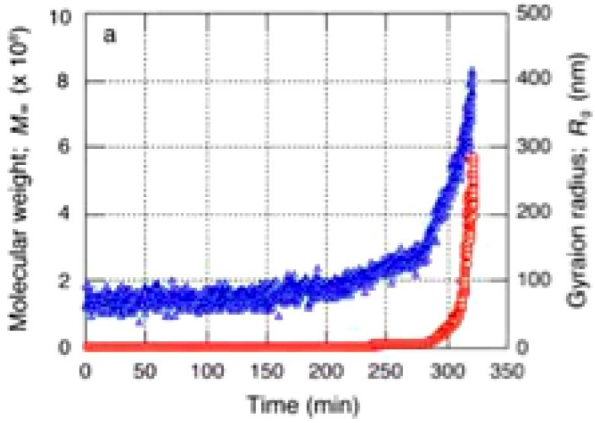

Fig. S3. Schematic representation of the direct transformation and heterogeneous growth models. (*A*) In the direct-transformation model, the transformation proceeds via internal compaction of a precursor (amorphous) particle, during which the gyration radius of the particle remains constant. (*B*) During heterogeneous growth transformation, the molecular mass, gyration radius, and fractal dimension increase simultaneously.

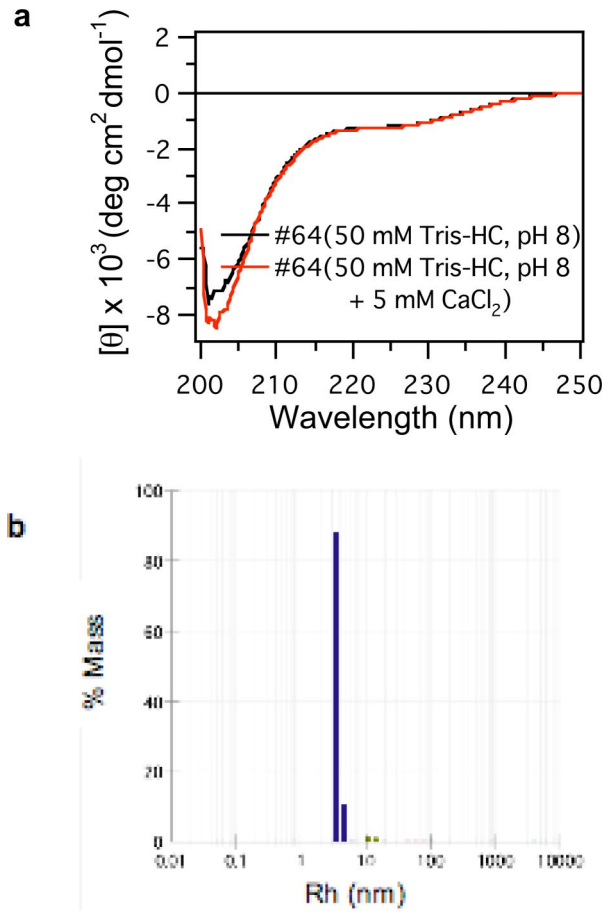

Fig. S4. TR-SLS measurements performed in the presence of 25 μg/ml of DMP1.

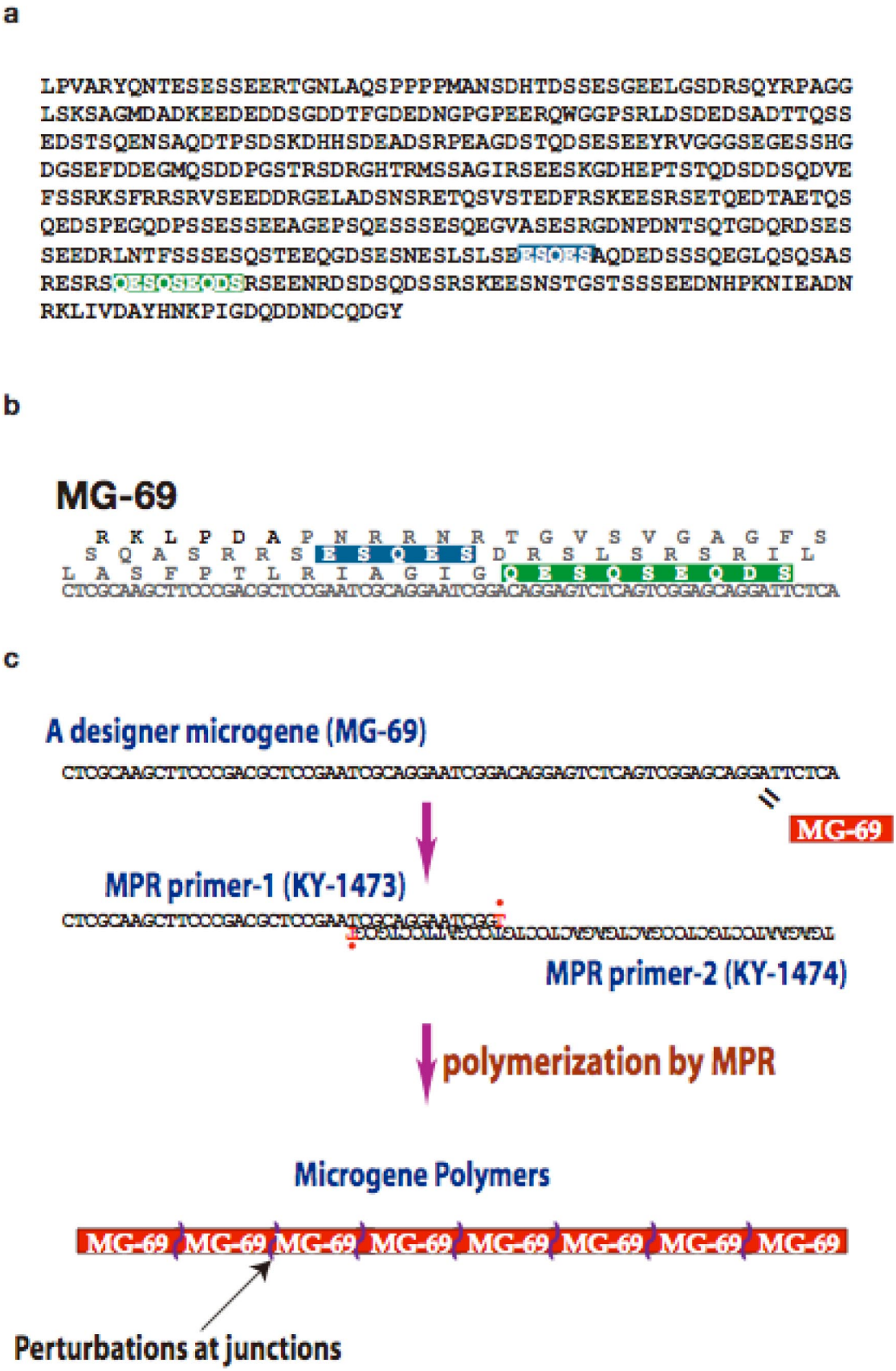

Fig. S5. CD spectra and DLS analysis of #64. (*a*) Far-UV CD spectra were measured in the absence (black) and presence (red) of 5 mM $CaCl_2$. (*b*) Size distributions of #64 are shown.

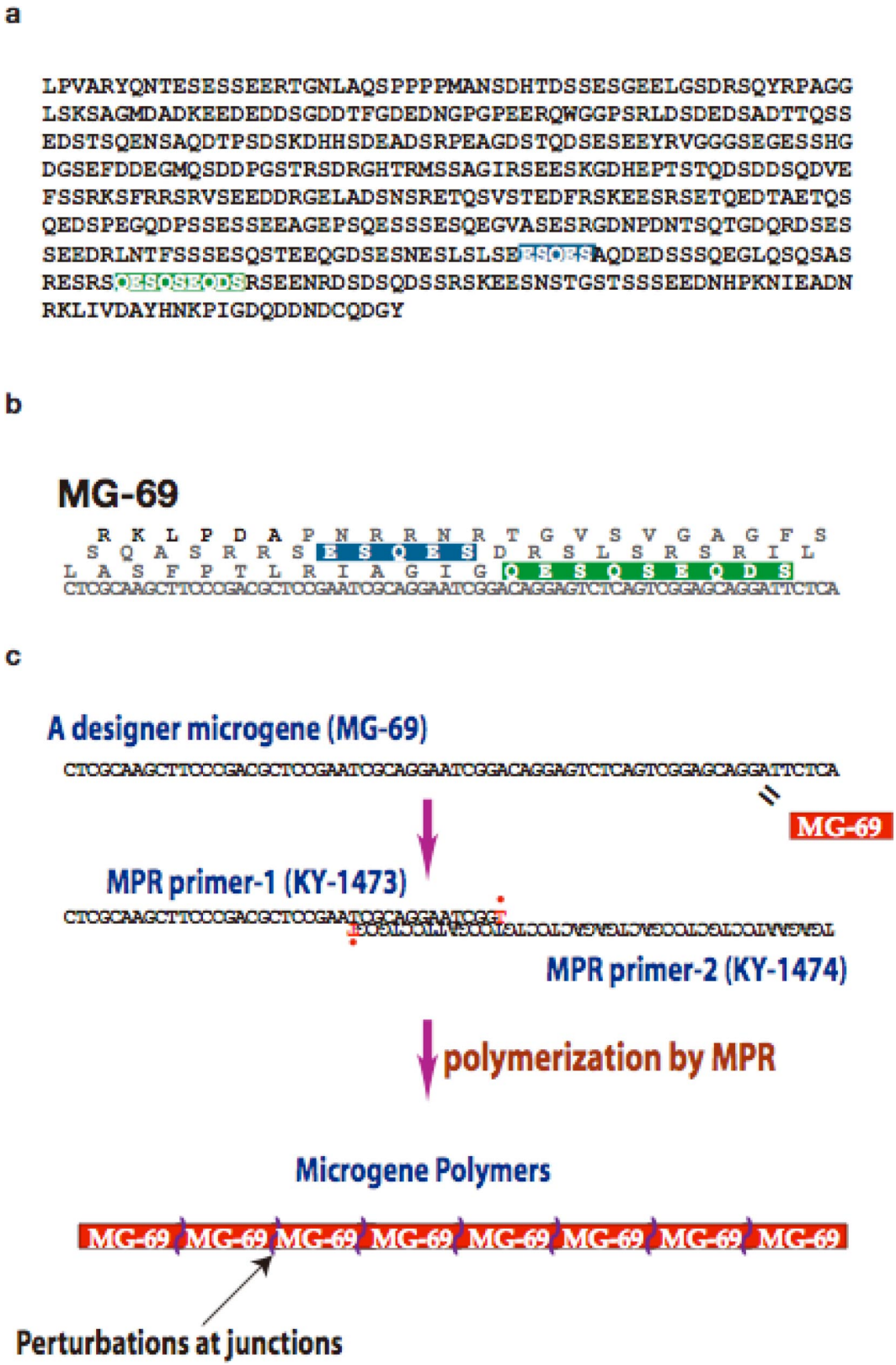

Fig. S6. The peptide sequence of DMP1 and the designer microgene that codes two DMP1 motif. (*a*) A Primary structure of DMP1 (11). Two acidic motifs that were previously shown to mediate nucleation during HAP formation (5) [motif A (ESQES) and motif B (QESQSEQDS)] are shown in blue and green letters, respectively. (*b*) The designer microgene used in this study, which encodes 3 peptide motifs in 3 different reading frames. The RKLPDA motif shown in black letters is the titanium-binding peptide minTBP-1 (6), which was not used in this study. (*c*) Scheme of the microgene polymerization reaction (MPR) (7, 8). Based on the microgene, 2 MPR primers with overlapping regions and a mismatched base pair at their 3′ ends were designed and synthesized. A thermal cycle reaction with the MPR primers resulted in the formation of microgene polymers. At junctions of the microgene, random insertions or deletions of nucleotides allowed combinatorial polymerization of the 3 reading frames encoded by the single microgene.

(a)

Fig. S7. Preparation of artificial proteins. (*a*) Primary structures of artificial proteins constructed in this study. Motif A and motif B are colored in blue and green, respectively. The amino acids substituted in the #64 mutants are underlined. The calculated molecular masses and pI values of the #64 mutants are also indicated. (*b*) SDS/PAGE of the purified artificial proteins. Molecular mass markers (14.4, 20.1, 30, 42.4, 66.3, and 97.4 Da) were run in the first lane.

♯64A[M.w.16.0kDa, pI 7.1]

MRGSHHHHHHTDPSTWADP
RRS*qSQqS*DRSLSRSRILT
RKLPDAPNRRNRTGVSVGAGFS
ASFPTLRIAGIGQESQSEQDS
LASFPTLRIAGIGQESQSEQDSH
ASFPTLRIAGIGQESQSEQDS
LASFPTLRIAGIGQESQSEGYPG

♯64B1[M.w.16.0kDa, pI 8.5]

MRGSHHHHHHTDPSTWADP
RRSESQESDRSLSRSRILT
RKLPDAPNRRNRTGVSVGAGFS
ASFPTLRIAGIGQqSQSqQnS
LASFPTLRIAGIGQESQSEQDSH
ASFPTLRIAGIGQESQSEQDS
LASFPTLRIAGIGQESQSEGYPG

♯64B2[M.w.16.0kDa, pI 8.5]

MRGSHHHHHHTDPSTWADP
RRSESQESDRSLSRSRILT
RKLPDAPNRRNRTGVSVGAGFS
ASFPTLRIAGIGQESQSEQDS
LASFPTLRIAGIGQqSqSqQnSH
ASFPTLRIAGIGQESQSEQDS
LASFPTLRIAGIGQESQSEGYPG

♯64B3[M.w.16.0kDa, pI 8.5]

MRGSHHHHHHTDPSTWADP
RRSESQESDRSLSRSRILT
RKLPDAPNRRNRTGVSVGAGFS
ASFPTLRIAGIGQESQSEQDS
LASFPTLRIAGIGQESQSEQDSH
ASFPTLRIAGIGQqSQSqQnS
LASFPTLRIAGIGQESQSEGYPG

(b)

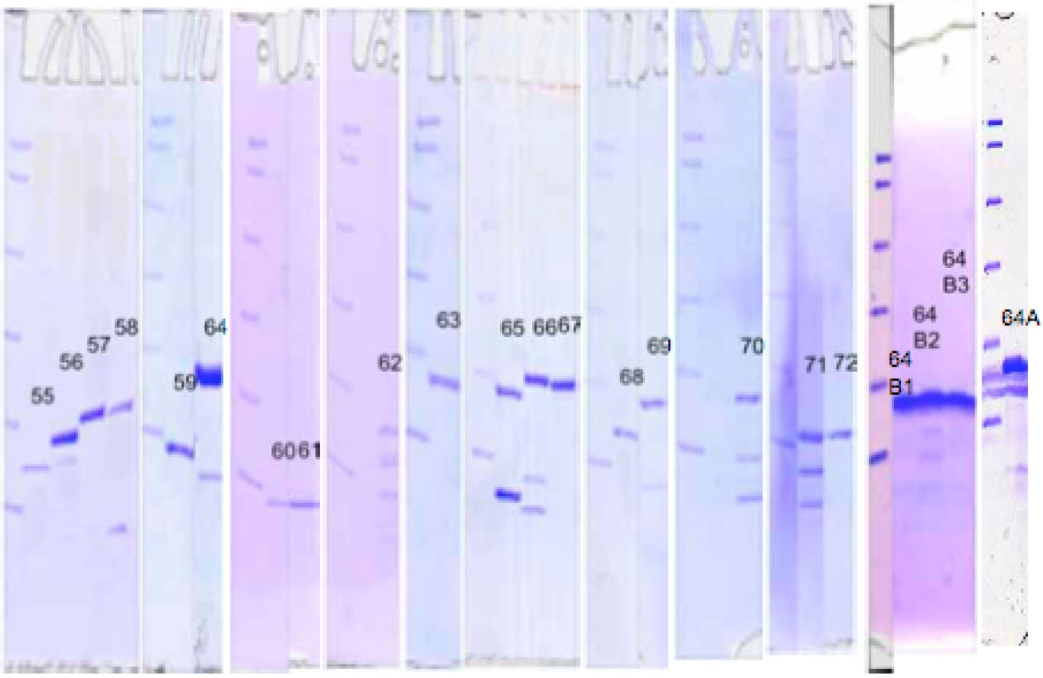

Fig. S7 ***continued.***

Table S1. Calcium phosphate precipitates formed in the presence of artificial proteins

	200 μg/ml	40 μg/ml	8 μg/ml	1.6 μg/ml
#64	None (7.1)	S. A. (6.6)	S. A. (6.6)	S. A. (6.9)
#68	None (7.1)	S. A. (6.9)	S. A. (6.7)	None (7.1)
#56	None (7.1)	None (7.1)	None (7.1)	None (7.1)
#69	None	None	None	None
#64A	S. A.	S. A.	None	None
#64B1	S. A.	None	None	None
#64B2	None	S. A.	None	None
#64B3	None	S. A.	None	None

Calcium phosphate aggregates were formed from a solution of 1.8 mM $CaCl_2$ and 1.08 mM KH_2PO_4 (pH7.4) in the presence of the indicated concentrations of protein. ″None″ indicates no precipitate was formed. ″S. A.″ indicates that the spherical OCP aggregates were formed after incubation for 5 days. The pH of the solution after incubation for 5 days is indicated in parentheses.

Table S2. Oligonucleotides used to construct the #64 mutants

	Part I		Part II		Part III	
	Templates	Primers	Templates	Primers	Templates	Primers
#64A	1–108(+)A	pri1–108(+)A	163–270(+)	pri163–270(+)	331–438(+)	pri331–438(+)
	79–186(−)	pri79–186(-)	247–357(−)	pri247–357(−)		pri331–438(+)r
#64B1	1–108(+)	pri1–1-108(+)	163–270(+)B1	pri163–270(+)	331–438(+)	pri331–438(+)
	79–186(−)	pri79–186(−)	247–357(−)	pri247–357(−)		pri331–438(+)r
#64B2	1–108(+)	pri1–108(+)	163–270(+)B2	pri163–270(+)	331–438(+)	pri331–438(+)
	79–186(−)	pri79–186(−)	247–357(−)B2	pri247–357(−)		pri331–438(+)r
#64B3	1–108(+)	pri1–1-108(+)	163–270(+)	pri163–270(+)	331–438(+)B3	pri331–438(+)B3
	79–186(−)	pri79–186(−)	247–357(−)B3	pri247–357(−)B3		pri331–438(+)r